# FAST IMPLEMENTATION OF HEAT RADIATION IN A SELF-CONSISTENT FDTD ANALYSIS TOOL FOR MICROWAVE AND HYBRID OVENS

J. Haala J. v. Hagen, Member W. Wiesbeck
*Institut für Höchstfrequenztechnik und Elektronik, Universität Karlsruhe*

*ABSTRACT. This paper presents an efficient simulation tool for conventional, microwave and combined heating. Two heat transfer mechanisms are included: conductive and radiant heat transfer. The conductive heat transfer is modeled by a finite difference algorithm. A modeling technique for radiant heat transfer in non-uniform grids has been developed and is here presented for the first time. A finite difference scheme is not applicable for the radiant heat transfer, as radiation from a material surface is not bounded to the immediate vicinity as is conductive heat transfer. Therefore ray optical methods are used. Rays connecting mutually visible surfaces are obtained by a new fast method. Necessary but acceptable simplifications allow fast computations. The algorithms are conveniently integrated together with an electromagnetic FDTD program into one simulation tool. Representative simulations are presented for an oven heated conventionally, by microwaves, and by a combination of both.*

## 1 INTRODUCTION

Thermal modeling is mandatory for the optimization of heating processes in ovens. Especially in combination with microwaves, the heating process has to be carefully designed to achieve fast and uniform heating. Various reports [1, 2, 3, 4, 5, 6, 7, 8, 9, 10] reported electromagnetic field computations of microwave ovens, but only few authors [11, 12] include in their procedures a thermal model. To the authors knowledge all models consider only the conductive heat transfer, radiation is usually neglected. This simplification becomes questionable at higher temperatures. In fact, with increasing temperature radiant heat exchange becomes more and more important, since the energy emitted from a material surface increases proportional to $T^4$. In contrast energy transported by heat conduction is only proportional to $T$. Radiant heat transfer eventually prevails conductive heat transfer. This paper specifically includes radiant heat transfer and therefore closes the gap of neglected radiant heat exchange.

Pure thermal problems are mostly simulated by Finite Element Programs [13], some of which include radiation. Heating by microwaves is sometimes considered, but the variation of the electromagnetic field with increasing temperature due to changing material properties is not. Additionally, these models normally perform only steady state calculations.

For the optimization of ovens one needs to determine the dynamic heat process. Hence, a combination of thermal and electromagnetic simulation must be used. Both radiation and the influence of increasing temperature on the electromagnetic field must be considered.

The Finite Difference Time Domain (FDTD) method has been found to be an excellent algorithm for the calculation of electromagnetic fields, especially in closed structures like ovens. This method needs less computational resources than methods in frequency domain. Broadband calculations are easily performed. The Finite Difference Time Domain modeling of thermal processes is also economical in memory usage. A combination with an electromagnetic FDTD leads to a very efficient and powerful simulation tool. Self-consistent modeling is possible as well as analyzing a dynamic heating process.

Both, the conductive thermal and electromagnetic algorithm are of local character as the temperature and the fields in one discretisation cell is only related to its neighbouring cells. This local scheme applies only to conductive heat transfer. When considering radiant heat transfer, energy may be transported through the whole computational space. Mutually visible surfaces, view factors and material parameters have to be determined and used for the calculation. This usually means high computational effort. However, the proposed method reduces this effort considerably.

The main task when including radiant heat transfer is to determine surface pairs being mutually visible and exchanging radiant energy. A very fast algorithm has been developed that is optimized for detecting mutually

visible surfaces in a rectangular non-uniform grid. This algorithm determines surface pairs very quickly. They need to be allocated and stored only once, before the calculation starts. After this initial step the calculation of the resulting temperature at each time step is very fast and easy.

After discussing the mechanism and the modeling of the conductive and radiant heat transfer, an efficient algorithm for the computation of view factors and transfer rays is presented. A next section shows the inclusion of the electromagnetic simulation. A hybrid oven simulation verifies the applicability of the method.

## 2 CONDUCTIVE HEAT TRANSFER

The finite difference scheme [14] is applied for the conductive heat transfer in a rectangular non-uniform grid with cells indexed by $(i, j, k)$. Inside a cell the temperature is assumed to be homogeneous. Heat flux density vectors describing the heat exchange with the neighbouring cells are defined in the middle of the six cell surfaces as shown in Fig. 1 for the discretisation cell $(i, j, k)$. The calculation of the temperature distribu-

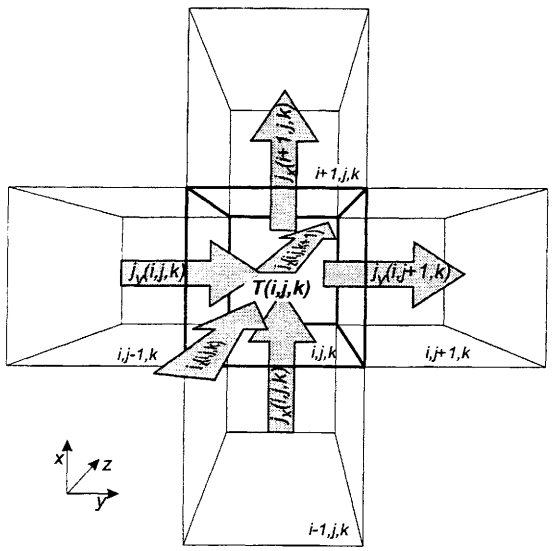


Figure 1: Discretisation cell $(i, j, k)$ and the position of the scalar field components $T$ and the vectors $\vec{j}$.

tion is divided into two steps. The heat flux densities are caused by the temperature gradients and given by

$$\vec{j}(\vec{x}, T) = -\sigma(\vec{x}, T)\ \mathrm{grad}\, T(\vec{x}, T) \qquad (1)$$

with $\vec{j}$ the heat flux density, and $\sigma$ the thermal conductivity. Considering only the $x$ component of $\vec{j}$ in Fig. 2, the gradient in equation (1) is expressed using the finite difference expression

$$\mathrm{grad}\, T(\vec{x}) = \frac{T(i,j,k) - T(i-1,j,k)}{\Delta x} \qquad (2)$$

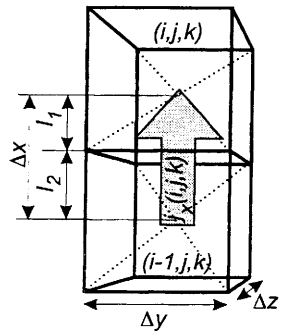


Figure 2: Geometrical properties for the calculation of the discretised field component $j_x$.

The thermal conductivity at $\vec{x}$ is the average of two neighbouring cells. With

$$\sigma(\vec{x}, T) = \Delta x \frac{\sigma(i,j,k)\,\sigma(i-1,j,k)}{l_2\sigma(i,j,k) + l_1\sigma(i-1,j,k)} \qquad (3)$$

one obtains

$$j_x(i,j,k) = \frac{\sigma(i,j,k)\,\sigma(i-1,j,k)}{l_2\sigma(i,j,k) + l_1\sigma(i-1,j,k)} \cdot (T(i-1,j,k) - T(i,j,k)) \qquad (4)$$

The thermal conductivity is assumed to be constant over the volume of one discretisation cell. As the heat flux density is supposed to be constant over the surface, the power $P_x$ flowing through the interface between the cells $(i, j, k)$ and $(i-1, j, k)$ is determined by

$$P_x(i,j,k) = \iint_A j_x\, dA = j_x(i,j,k)\,\Delta y \Delta z \qquad (5)$$

All other components of $\vec{j}$ and $P$ are obtained accordingly.

The next step is the application of the conservation of energy. The change of temperature within a discretisation cell is derived from the change of energy. When the conservation of energy

$$\mathrm{div}\vec{j}(\vec{x}, T) + c_v(\vec{x}, T)\ \rho(\vec{x}, T)\ \frac{\delta}{\delta t} T(\vec{x}) = 0 \qquad (6)$$

is applied to one cell $(i, j, k)$ the divergence of $\vec{j}$ equals the power that flows through the surfaces of the cell. $c_v$ and $\rho$ are the specific heat capacity and the density, respectively. The divergence of $\vec{j}$ is expressed by the discretised surface integral in equation (5).

$$\begin{aligned} &\mathrm{div}\, j(\vec{x}) \Rightarrow \qquad (7)\\ &\oiint_A j(\vec{x})\, dA = (P_x(i,j,k) - P_x(i+1,j,k) \\ &\quad + P_y(i,j,k) - P_y(i,j+1,k) \\ &\quad + P_z(i,j,k) - P_z(i,j,k+1)) \end{aligned}$$

in the finite difference scheme.

The right hand side term in equation (6) applied to the cell volume leads to

$$c_v(\vec{x},T)\ \rho(\vec{x},T)\ \frac{\delta}{\delta t}T(\vec{x}) \Rightarrow \tag{8}$$
$$\iiint_V c_v(\vec{x},T)\ \rho(\vec{x},T)\ \frac{\delta}{\delta t}T(\vec{x})\ dV =$$
$$\Delta x\,\Delta y\,\Delta z\ c_v(i,j,k)\ \rho(i,j,k)\ \frac{\delta}{\delta t}T(i,j,k)$$

Finally the time derivative is also expressed by a finite difference

$$\frac{\delta}{\delta t}T(\vec{x}) = \frac{T^{n+1}(i,j,k) - T^n(i,j,k)}{\Delta t} \tag{9}$$

where $T^n$ denotes the temperature at time step $n$. Using equations (7), (8) and (9) one obtains

$$\begin{aligned} T^{n+1}(i,j,k) &= T^n(i,j,k) + \\ &\frac{\Delta t}{\Delta x\,\Delta y\,\Delta z\ c_v(i,j,k)\ \rho(i,j,k)} \cdot \\ &(P_x(i,j,k) - P_x(i+1,j,k) + \\ &P_y(i,j,k) - P_y(i,j+1,k) + \\ &P_z(i,j,k) - P_z(i,j,k+1)) \end{aligned} \tag{10}$$

With equations (4) and (10) the temperature is updated at each time step. The time step $\Delta t$ has to be chosen carefully, since instabilities may arise. The algorithm is stable for

$$\Delta t \le \frac{c_v \rho}{2\sigma}\,\Delta x^2 \tag{11}$$

where $\Delta x$ is the discretisation with [14]. Equation (11) has to be satisfied for every discretisation cell.

## 3 RADIANT HEAT TRANSFER

With increasing time in the simulation the increase of temperature may cause a variation of the electric and thermal properties, but the geometry remains constant. Therefore geometry checks are performed only once before calculation starts. The checks include the determination of radiant surfaces, testing for visibility and the calculation of view factors.

The radiant heat transfer only applies to interfaces between solid and gaseous materials. Therefore the first step is to determine those surfaces within the finite difference grid. The surfaces of the solids are assumed to be rough. The Stefan-Boltzmann and Lambert equations determine for this case the specific heat radiation

$$M = \frac{A}{\pi}\varepsilon\ \cos\theta\ \sigma T^4 \tag{12}$$

of a surface $A$ oriented in a coordinate system according to Fig. 3 at temperature $T$ in direction $\varphi$ and $\theta$.

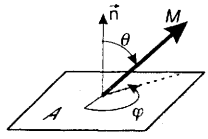


Figure 3: Specific thermal radiation of a surface $A$.

$\sigma$ is the Stefan-Boltzmann constant, and $\varepsilon$ represents the relation between the emission of the real surface compared to a black emitter. Obviously, the radiation only depends on the elevation angle $\theta$ and not on the azimuth angle $\varphi$ because of radial symmetry.

In closed environments like ovens, all the radiated energy is absorbed by other surfaces. For the calculation of the radiant heat all energy exchanges between surfaces have to be calculated. As shown in Fig. 4 the

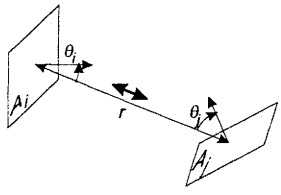


Figure 4: Radiation between two rectangular planes.

radiation of surface $A_i$ is partially absorbed by surface $A_j$. The absorbing surface $A_j$, however, also emits thermal radiation. A part of this radiation is in turn absorbed by $A_i$. The power exchanged between the two surfaces $i$ and $j$ is

$$P_{\text{rad}} = \Phi_{ij} - \Phi_{ji} \tag{13}$$

where

$$\begin{aligned} \Phi_{ij} &= A_i\,\varepsilon_i\,\alpha_j\,F_{ij}\,\sigma_i\,T_i^4 \\ \Phi_{ji} &= A_j\,\varepsilon_j\,\alpha_i\,F_{ji}\,\sigma_j\,T_j^4 \end{aligned} \tag{14}$$

where $\alpha_i$ and $\varepsilon_i$ are the absorption and emission coefficient of surface $A_i$, respectively. Kirchhoff's law states that $\alpha_i$ equals $\varepsilon_i$. The view factors $F_{ij}$ and $F_{ji}$ are coefficients determined by the geometry only. They express the part of energy that is transmitted by surface $A_i$ and actually received by surface $A_j$, divided by the total energy emitted by surface $A_i$. The view factors $F_{ij}$ are given by

$$F_{ij} = \frac{1}{\pi\,A_i}\int_{A_i}\int_{A_j}\frac{\cos\varphi_i\ \cos\varphi_j}{r^2}dA_j\,dA_i \tag{15}$$

and are determined by geometrical properties as shown in Fig. 4. The factors have values between 0 for infinitesimal surfaces infinitely separated and 1 for two

parallel, infinitely extended planes. The $F_{ij}$ are constant with respect to temperature.

The final temperature distribution is determined by the energy exchange between all surfaces. The radiant power flowing through the surfaces of cell $(i, j, k)$ is now used to calculate the variation of the temperature. When applying the conservation of energy, equation (6), to the radiant heat transfer one finally obtains

$$T^{n+1}(i,j,k) = T^{n}(i,j,k) + \frac{\Delta t}{\Delta x\,\Delta y\,\Delta z\; c_v\,(i,j,k)\;\rho\,(i,j,k)} \cdot \sum_{\text{Surface}} P_{\text{rad}} \tag{16}$$

For maximum versatility, the simulations are based on a cartesian, but non-uniform grid. This allows an enormous simplification for the determination of view factors. An efficient calculation is obtained if the geometrical properties are checked and the view factors calculated and stored only once before the calculation starts. During the calculation the stored values are simply processed in a look-up table.

The preprocessing is divided into two steps. First the relevant cells are determined. Only cells representing solid materials bordered by a gas or vacuum are relevant as only those cells radiate or absorb energy.

The next step is to determine surface pairs. Two surfaces are called a surface pair when they exchange energy. Energy exchanges only apply to surfaces that are mutually visible. Every possible combination of surfaces has to be checked whether they are linked by a line of sight. Depending on the size and properties of the oven and the discretisation millions of possible surface pairs exist. Hence, the visibility check has to be very efficient.

Here a modified Bresenham algorithm is used which combines versatility and efficiency. Fig. 5 shows two surfaces that are checked whether they are mutually visible. A virtual line connects the surface centers. If each cell penetrated by the connecting line is gaseous then the surfaces are mutually visible. Computer graphics use Bresenham algorithms [15, 16] to draw lines on a screen. This algorithm determines very fast the pixels that are penetrated by a line. However, this algorithm has been developed for two dimensional uniform grids. Here the algorithm is extended to three dimensional non-uniform grids.

The check starts from one surface and proceeds along the connecting line. The first penetrated cell is the one directly attached to the surface. To determine which cell is penetrated next the distances $l_x$, $l_y$ and $l_z$ in Fig. 5 are calculated. These are the distances along the connecting line until a new cell in $x$, $y$ or $z$ direction is

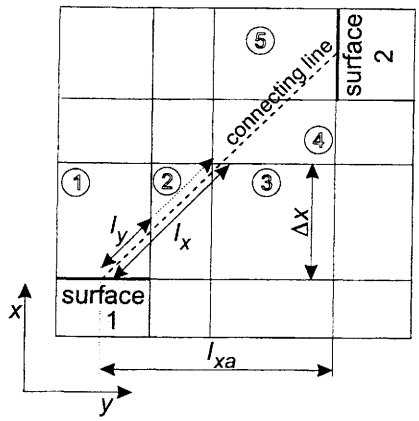


Figure 5: Two dimensional Bresenham algorithm in a non-uniform grid.

reached. The distance $l_x$ is calculated by

$$l_x = \Delta x \sqrt{1 + \frac{l_{ya}^2 + l_{za}^2}{l_{xa}^2}} \tag{17}$$

where $\Delta x$ is the minimum distance in $x$ direction to the next cell. $\Delta x$ is normally the cell width and therefore easily accessible. $l_{xa}$, $l_{ya}$ and $l_{za}$ are the overall distances between the surface centers in $x$, $y$ and $z$ direction, respectively. $l_y$ and $l_z$ are also calculated according to equation (17).

The minimum of $l_x$, $l_y$ and $l_z$ determines if the next penetrated cell is in $x$, $y$ or $z$ direction. In our example in Fig. 5 the next cell is reached in $y$ direction. This cell is tested if it is still gaseous. Then $l_y$ is increased by

$$l_y = l_y + \Delta y \sqrt{1 + \frac{l_{xa}^2 + l_{za}^2}{l_{ya}^2}} \tag{18}$$

where $\Delta y$ is the new cell width. The square root term on the right hand side is constant and is calculated only once. In comparison to the original algorithm only one additional multiplication of the term in the square root with the actual cell width $\Delta y$ is needed. This is due to the non-uniformity of the grid.

The determination of the penetrated cells is continued until a cell with solid material, or the second surface of interest is reached. In the first case, the surfaces are not mutually visible.

The algorithm only determines whether there is a line of sight or not. Partial visibility is not considered, since the computational effort would be very high. However, as the discretised surfaces are normally very small, only a slight error arises.

For each surface pair the view factors $F_{ij}$ are calculated. Using the reciprocity

$$A_i F_{ij} = A_j F_{ji} \tag{19}$$

the view factors are calculated only once for each surface pair. As the surfaces are either parallel or perpendicular oriented in the rectangular grid, the integrals in equation (15) can be simplified. [17] showed a method for evaluating the view factor without integration making the calculation much faster.

## 4 MICROWAVE HEATING

The heating of materials by microwaves is determined directly using

$$P_{\text{elec}} - \iiint_V c_{\text{v}}(\vec{x},T)\ \rho(\vec{x},T)\ \frac{\delta}{\delta t}T(\vec{x},T)\ dV = 0 \quad (20)$$

where $P_{\text{elec}}$ is the microwave power dissipated. As shown in Fig. 6 there are twelve electric field components dissipating power within one cell. The electromagnetic power

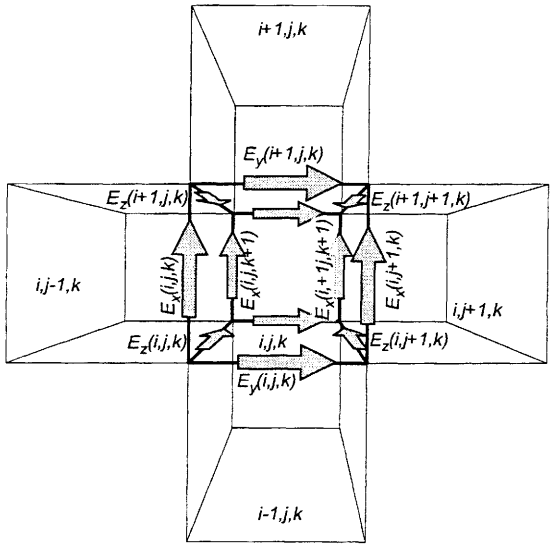


Figure 6: Placement of the electric field components within the discretisation cell $(i,j,k)$.

$$P_{\text{elec}} = \frac{\Delta x\,\Delta y\,\Delta z}{4}\sum_{n=1}^{12}\kappa\,|E_n|^2 \quad (21)$$

is determined by the conductivity $\kappa$ of the material . Combining (20) and (21) and setting up the finite difference scheme one obtains

$$T^{n+1}(i,j,k) = T^n(i,j,k) + \frac{\Delta t}{4c_{\text{v}}(i,j,k)\ \rho(i,j,k)}\cdot\sum_{n=1}^{12}\kappa\,|E_n|^2 \quad (22)$$

The computation of the electric energy dissipated in one cell is done by a standard FDTD scheme, and includes linear and frequency-dependent materials.

Additionally, equations (7), (16), and (22) are combined to update the temperature in only one computational step. The radiant, conductive and electric power is summed up leading to

$$T^{n+1}(i,j,k) = T^n(i,j,k) + \frac{\Delta t}{\Delta x\,\Delta y\,\Delta z\ c_{\text{v}}(i,j,k)\,\rho(i,j,k)}\cdot\left(\sum_{\text{Surface}}P_{\text{rad}} + \sum_{\text{Surface}}P_{\text{cond}} + \sum_{\text{Volume}}P_{\text{elec}}\right) \quad (23)$$

## 5 SIMULATION OF A HYBRID OVEN

In this section the above method is applied to the simulation of a hybrid oven loaded with material samples. The oven has the dimensions $400 \times 360 \times 350\text{mm}^3$ and is sketched in Fig. 7.

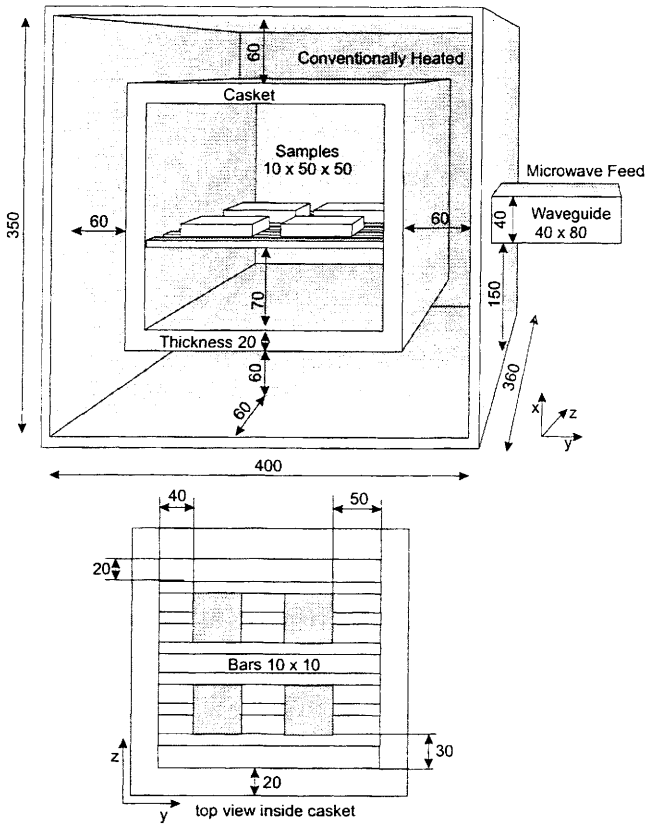


Figure 7: Hybrid oven with casket and samples inside. The samples are placed on bars. The front and rear wall are heated conventionally. Dimensions in mm.

The oven is descretised using 34850 discretisation

Table 1: Material Parameters used in the Simulation

| Material | Parameter | Value | $T$ in K |
|---|---|---|---|
| Samples | Specific | 765 | 300 |
| | Heat $c_v$ | 940 | 400 |
| | | 1110 | 600 |
| | Density $\rho$ | 3970 | 0-1000 |
| | Thermal | 36 | 300 |
| | Cond. $\sigma$ | 27 | 400 |
| | | 16 | 600 |
| | | 10 | 1000 |
| | Emission-, | 0.78 | 400 |
| | Absorption- | 0.69 | 600 |
| | Coeff. $\varepsilon = \alpha$ | 0.61 | 800 |
| | | 0.51 | 1000 |
| | Rel. Perm. $\varepsilon_{el}$ | 9.6 | 0-1000 |
| | Cond. $\kappa$ | 0.5 | 0-1000 |
| Casket | same as samples except | | |
| +bars | Conductivity $\kappa$ | 0.1 | 0-1000 |
| Oven | Thermal Cond. $\sigma$ | 138 | 0-1000 |
| (Carbon) | Emission-Coeff. $\varepsilon$ | 0.29 | 0-1000 |
| | Conductivity $\kappa$ | 105 | 0-1000 |

Units: $[c_v]$ = J/kgK, $[\rho]$ = kg/m$^3$, $[\sigma]$ = W/mK, $[\varepsilon, \alpha] = 1$, $[\varepsilon_{el}]$ = As/Vm, $[\kappa]$ = S/m

cells for the thermal model. For the electromagnetic modelling 66400 cells are used. The discretisation differs in the areas where air is present as for thermal modelling a course mesh is used. For areas filled with materials the same discretisation is used for thermal and electromagnetic modelling. 3 Mio. surface pairs which exchange radiant heat transfer are detected within the structure. The determination of them takes 85s on an HP workstation C240. The calculation of the electromagnetic field and the 600s heating period lasts 200s and 40min, respectively. To model the oven 90MB computational memory is needed.

The walls of the oven consist of Carbon. Inside the oven an $Al_2O_3$ casket carries four samples on $Al_2O_3$ bars. The electromagnetic and thermal material parameters of the casket and the samples are summarized in Tab. 1.

### 5.1 Conventional Heating

The front and rear wall of the oven are heated conventionally to a constant temperature of 2000K. Computational results are given in Fig. 8 for $t$ = 0s, $t$ = 240s and

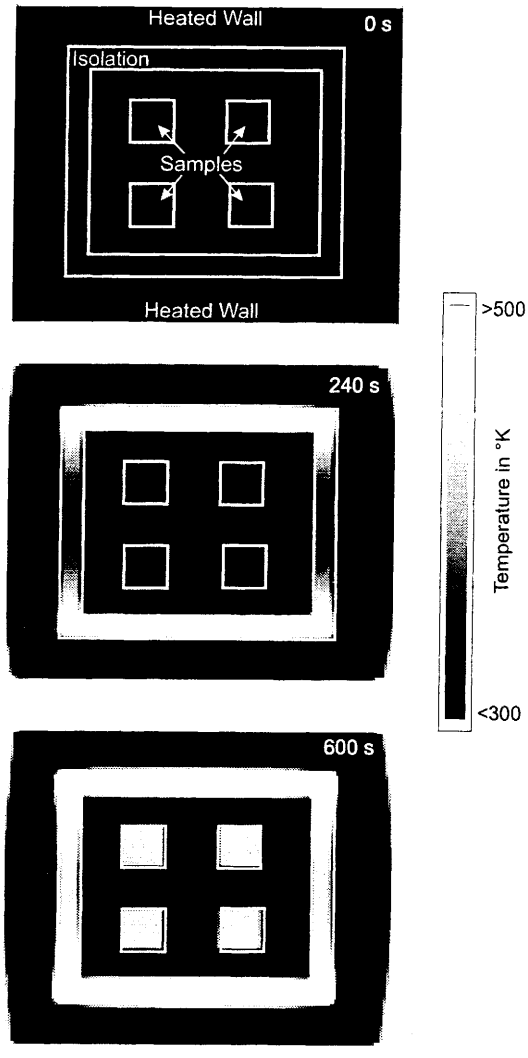


Figure 8: Results for the conventional heating at time steps $t$ = 0s, $t$ = 240s and $t$ = 600s for a view plane at $x$ = 165mm

$t$ = 600s. One observes that first the casket is heated by radiation of the hot walls. The energy is then transported inwards through the casket walls by conduction. Once the interior of the casket is heated up, the samples are heated by radiation from the casket. A closer look at the temperature distribution inside a single sample is shown in Fig. 12. A discussion of the distribution is given below.

### 5.2 Microwave Heating

The microwave power is fed through a waveguide with dimensions 80 × 40mm$^2$ located in the middle of a side wall. The generator has a frequency of 2.45GHz and

produces 1.5kW microwave power. In Fig. 9 the electromagnetic field distribution at $f = 2.45$GHz in the fre-

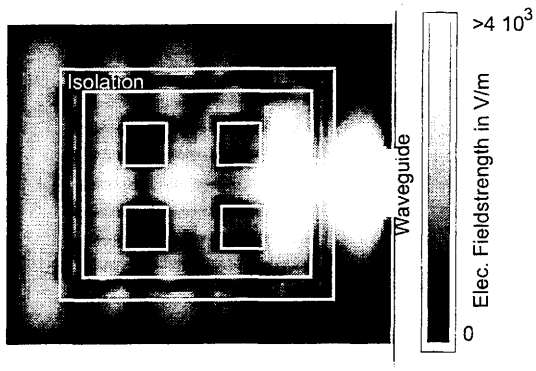


Figure 9: Electric field strength within the oven for a view plane at $x = 165$mm

quency domain is given in a view plane at $x = 165$mm. Clearly seen are the resonances arising within the casket.

In Fig. 10 the temperature distribution is given for

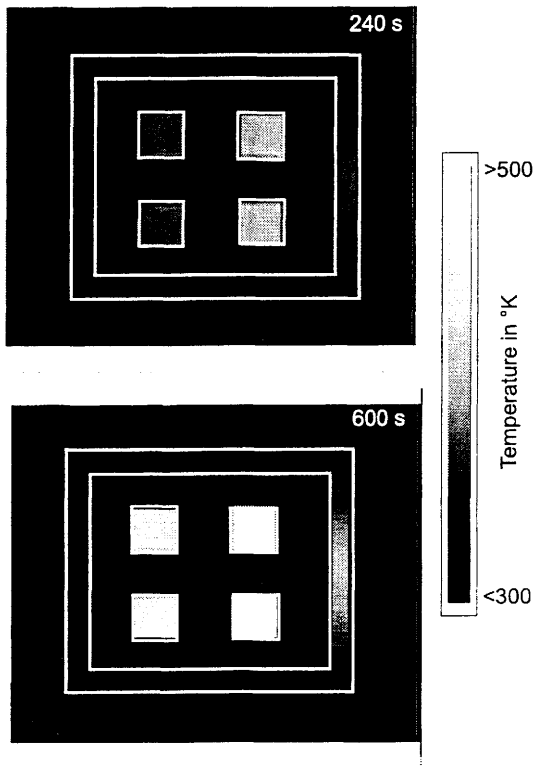


Figure 10: Results for the microwave heating at time steps $t = 240$s and $t = 600$s for a view plane at $x = 165$mm

240s and 600s. The samples near the feed are heated faster.

### 5.3 Hybrid Heating

The results of the combination of both heat sources look similar to a linear superposition of the heating patterns of the single heat sources (Fig. 11). However, the power of the single sources need to be adjusted. A quasi-

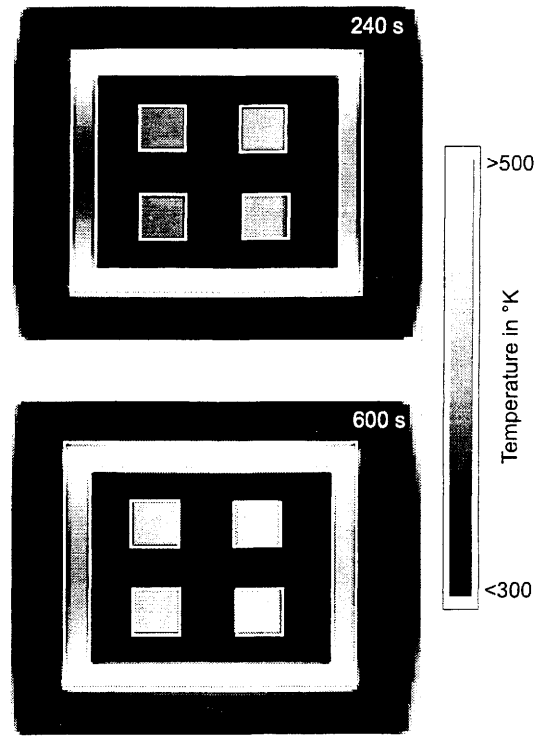


Figure 11: Results for the hybrid heating at time steps $t = 240$s and $t = 600$s for a view plane at $x = 165$mm

optimal heating was achieved for 800W microwave power. The microwaves are heating the samples nearly uniformly. If the interior side of the casket is kept at the same temperature as the samples, the exterior of the samples remain at the same temperature as the interior. This is considered to be the best performance.

### 5.4 Temperature distribution inside a sample

The upper left sample in Figs. 8-11 is shown enlarged in Fig. 12 for the three different types of heating at time $t = 240$s. The distributions are calculated and shown in a horizontal cut in the middle of the sample. To see the temperature differences in the sample more clearly a normalization is used. The colortable is adjusted to temperature span inside the sample. The absolute values are given for each temperature plot.

In the left two figures showing the temperature distribution for conventional and microwave heating with 800W microwave power one can see clearly a temperature gradient. It is also obvious that the microwave

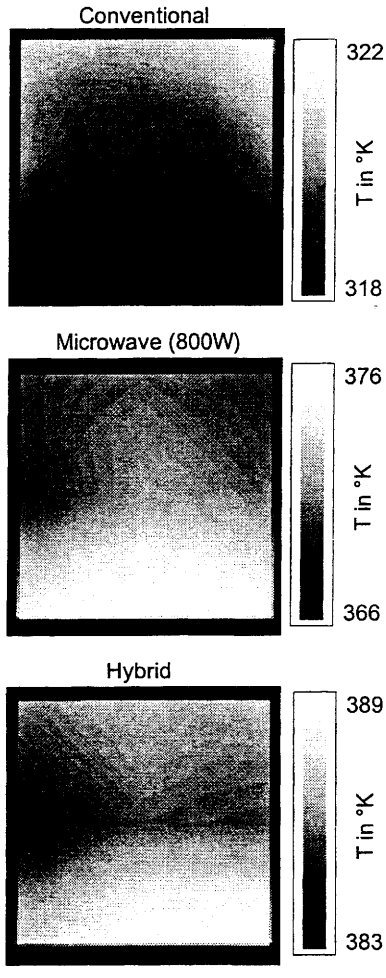


Figure 12: Temperature distribution within the upper left sample at time $t = 240$s. The colortables are adjusted to the temperature span within the samples.

heating produces a higher heating rate at this paper. The hybrid heating leads to a more homogeneous and faster warm up than the single heat sources. However, if desired one could also optimize for a temperature gradient or any other heat pattern.

## 6 CONCLUSION

A new method was presented to simulate heating processes including thermal energy exchanges by conduction and radiation. The algorithms are implemented within an electromagnetic FDTD-code, allowing the calculation of conventionally heated and microwave ovens. For the conductive heat transfer a finite difference scheme is used. Ray optical methods are introduced to check visibility of surfaces and consequently the possibility of radiant heat exchange. The resulting simulation tool is very powerful and mandatory to design high quality ovens. It allows the determination of temperature distribution inside materials and an optimization for any desired heat pattern. Especially for hybrid ovens where different heat sources have to be adjusted, the developed software package has been proven to offer an excellent opportunity to simulate heating processes and to support hybrid oven designs.

## REFERENCES

[1] T. V. Chow Ting Chan and H. C. Reader, "Modelling of modes and perspectives on multiple-feeds in microwave ovens," *Journal of Microwave Power and Electromagnetic Energy*, vol. 31, no. 4, pp. 238–250, 1996.

[2] W. Fu and A. Metaxas, "Numerical prediction of three-dimensional power density distribution in a multi-mode cavity," *Journal of Microwave Power and Electromagnetic Energy*, vol. 29, no. 2, pp. 67–75, 1994.

[3] M. F. Iskander, R. L. Smith, A. Octavio, M. Andrade, H. Kimrey, and L. M. Walsh, "FDTD simulation of microwave sintering of ceramics in multimode cavities," *IEEE Trans. on Microwave Theory and Techniques*, vol. 42, pp. 793–800, may 1994.

[4] K. Iwabuchi, T. Kubota, and T. Kashiwa, "Analysis of electromagnetic fields in a mass-produced microwave oven using the finite-difference time-domain method," *Journal of Microwave Power and Electromagnetic Energy*, vol. 31, no. 3, pp. 188–196, 1996.

[5] G. A. Kriegsmann, "Cavity effects in microwave heating of ceramics," *Siam Journal of Applied Mathematics*, vol. 57, pp. 382–400, april 1997.

[6] F. Liu, I. Turne, and M. Bialkowski, "A finite-difference time-domain simulation of power density distribution in a dielectric loaded microwave cavity," *Journal of Microwave Power and Electromagnetic Energy*, vol. 29, no. 3, pp. 138–148, 1994.

[7] M. Subirats, M. F. Iskander, M. J. White, and J. O. Kiggans, Jr., "FDTD simulation of microwave sintering in large (500/4000 liter) multimode cavities," *Journal of Microwave Power and Electromagnetic Energy*, vol. 32, no. 3, pp. 161–170, 1997.

[8] S. Sundberg, P. Kildal, and T. Ohlsson, "Moment method analysis of a microwave tunnel oven," *Journal Microwave Power and Electromagnetic Energy*, vol. 33, no. 1, pp. 36–48, 1998.

[9] H. Zhao and I. W. Turner, "An analysis of the finite-difference time-domain method for modeling the microwave heating of dielectric materials within a three-dimensional cavity system," *Journal of Microwave Power and Electromagnetic Energy*, vol. 31, no. 4, pp. 199–214, 1996.

[10] H. Zhao and I. W. Turner, "A generalized finite-volume time-domain algorithm for microwave heating problems on arbitrary irregular grids," *13th Annual Review of Progress in Applied Computational Electromagnetics*, vol. 31, pp. 199–214, march 1996.

[11] F. Torres and B. Jecko, "Complete FDTD analysis of microwave heating processes in frequency-dependent and temperature-dependent media," *IEEE Trans on Microwave Theory and Techniques*, vol. 45, pp. 108–117, january 1997.

[12] L. Ma, D.-L. Paul, N. Pothecary, C. Railton, J. Bows, L. Barratt, J. Mullin, and D. Simons, "Experimental validation of a combined electromagnetic and thermal FDTD model of a microwave heating process," *IEEE Trans. on Microwave Theory and Techniques*, vol. 43, pp. 2565–2571, november 1995.

[13] H.-C. Huang and A. S. Usmani, *Finite Element Analysis for Heat Transfer.* Heidelberg: Springer Verlag, 1994.

[14] M. Shashkow, *Conservative Finite-Difference Methods on General Grids.* CRC Press, 1996.

[15] B. Zalik, G. Clapworthy, and C. Oblonsek, "An efficient code-based voxel-traversing algorithm," *Computer Graphics Forum*, vol. 16, pp. 119–147, june 1997.

[16] C. Yuesheng and C. Zhenchu, "The bresenham's line algorithm line algorithm in multi-dimension," *Proceedings of the 4th Int. Conf. on Computer-Aided Drafting, Design and Manufacturing Technology*, pp. 133–139, august 1994.

[17] C. Hsu, "Shape factor equations for radiant heat transfer between two arbitrary sizes of rectangular planes," *Canadian Journal Chem. Eng.*, vol. 45, 1967.